

POTENTIAL VOLUMIZING EFFECT OF THE POST-MORPH LIME FILLER IN ATTENUATING CONCRETE CARBONATION

MUHAMAD HASIF HUSSIN¹, MOHD HAZIMAN WAN IBRAHIM^{1*},
NOR HAZURINA OTHMAN², MOHAMMED YAHYA MOHAMMED AL-FASIH³,
AND MOHD FADZIL ARSHAD⁴

¹*Jamilus Research Center, Faculty of Civil Engineering and Built Environment,
Universiti Tun Hussein Onn Malaysia, Batu Pahat, Johor, Malaysia*

²*Department of Civil Engineering, Faculty of Civil Engineering and Built Environment,
Universiti Tun Hussein Onn Malaysia, Batu Pahat, Johor, Malaysia*

³*School of Civil Engineering, Faculty of Engineering, Universiti Teknologi Malaysia,
Skudai, Johor, Malaysia*

⁴*Faculty of Civil Engineering, Universiti Teknologi MARA (UiTM),
Shah Alam, Selangor, Malaysia*

*Corresponding author haziman@uthm.edu.my

(Received: 16th January 2021; Accepted: 13th October 2021; Published on-line: 4th January 2022)

ABSTRACT: A study on the crystallography of the lime that comes from mussel shell has been conducted to determine the packing density of the material. The experimental analysis encompasses of concrete samples preparation with lime replacement at 5%, 7.5% and 10% by cement weight. The samples were carbonised naturally over a period of six months and subjected to the phenolphthalein test at 60, 90, 120 and 180 days. It has been found that lime originating from the mussel shell is of both the aragonitic and calcitic crystal types. Both crystal polymorphs of aragonite and calcite are denser than the typical normal concrete by 27.8% and 18.3% respectively. This suggest a volumizing effect that is beneficial to reduce carbonation penetration into the capillarity of the concrete. Results from the carbonation test indicate that concrete containing mussel shell lime ash showed up to 51% lower carbonation coefficient and significantly lower intensity of capillarity as shown via FESEM.

ABSTRAK: Kajian mengenai kristalografi kapur yang didapati daripada kulit kupang telah dijalankan bagi menentukan kepadatan bahan tersebut. Analisis eksperimen merangkumi penyediaan sampel-sampel konkrit yang mengandungi gantian kapur pada 5%, 7.5% dan 10% daripada berat simen. Sampel-sampel telah dikarbonatkan secara alami selama enam bulan dan menjalani ujian fenolftalin pada usia 60, 90, 120 dan 180 hari. Kajian telah mendapati bahawa kulit kupang terdiri daripada kapur-kapur berjenis aragonit dan kalsit. Kedua-dua polimorf kapur aragonit dan kalsit adalah 27.8% dan 18.3% lebih tumpat berbanding konkrit biasa. Hal ini berpotensi menjadi bahan penumpat yang bagus untuk mengurangkan serapan pengkarbonatan ke dalam kapilari konkrit. Keputusan ujian pengkarbonatan menunjukkan konkrit yang mengandungi abu kapur kulit kupang mempunyai pekali pengkarbonatan sehingga 51% lebih rendah dan mempunyai kerendahan kapilariti yang signifikan seperti yang ditunjukkan melalui FESEM.

KEYWORDS: *mussel shell ash; natural carbonation; calcium carbonate crystal*

1. INTRODUCTION

Concrete carbonation leads to the precipitation of lime (calcium carbonate) in the pores and this can either be advantageous or problematic, depending on the involved situation. In practice, some civil engineering structures such as mass concrete and girders take advantage of the carbonation process through the densifying property of the lime which can reduce the porosity of concrete. Several researchers such as Sideris [1], Phung et al. [2] and Rezvani [3] have indicated the pro-filler attribute of using lime in concretes.

Carbonation is notoriously known to cause serviceability issue in reinforced concretes. When the embedded steel reinforcement corrodes due to carbonation of concrete, the steel expanded in volume which causes the concrete cover to spall. This can expose the embedded steel and deeper part of the concrete to various other chemical and physical attacks apart from the costly repair. According to Ekolu [4], global corrosion related damage cost is at about 3-4% of the global gross domestic product (GDP). These 3-4% out of the GDP figure is accumulative of various industries and not limited to construction alone. However, Shibata [5] highlighted that buildings and infrastructures sectors had contributed a staggering 38% out of the global 3-4% figure which summed up to one trillion US dollars.

Many research and methods were imposed to counter concrete carbonation ever since and this include but not limited to increasing concrete cover (most common) in the range of 25-30 mm as suggested by Benitez [6] and Nakai [7], using well known substances such as fly ash [8-21], slag [12,13,20,22-24], lime [1,8-10,16,20,25-35] and even using commercial rust inhibitor [36,37]. It has been found that by using cover depth of 25-30 mm, the concrete service life increased significantly. However, there are also several case studies that have been conducted [38,39] which indicated that over-reliance on concrete cover thickness will not suffice. Possan [38] study indicated that the mean carbonation depth of the thirty-five years old concrete structure is 33.0 ± 6.6 mm. Whereas, Oliveira and Nogueira [39] study indicated mean carbonation depths for the thirty-one years old concrete structure varied from 54.01-104.83 mm. These are already beyond the limit of the suggested thickness in the previous studies. Since the typical and minimum design life of common concrete structures is fifty-years old and can go a maximum of one-hundred years if it is civil engineering structures such as in [38] and [39], the covers indeed underperformed in both cases. Thicker concrete cover requires more material, more space allocations and needless to say, bigger budget. None of these are ideal when it comes to modern projects with complex structural twist in the design that may limit available space for extra cover thickness and the typical demand for “minimum cost, maximum output”.

Fly ash is a very common material used in the industry to cater for special needs in terms of engineering aspect. Unfortunately, carbonation studies incorporating fly ash [8, 11,12-14,18-21] at various percentages indicated a trend that is prone to anti-filler effect when it comes to concrete carbonation. About only twenty-two percent of the studies indicated increased in carbonation resistance [10,12,15,16], sixty-seven percent indicated decreased in carbonation resistance [8,11,12-14,18-21] and eleven percent indicated as unresponsive variable [9,17]. The issue with fly ash is that it increases the concrete porosity and this is verified through the extended x-ray (XRAM) and Mercury Intrusion Porosimetry (MIP) methods as discussed in [18]. Concrete containing slags showed no better improvement in terms of carbonation resistance either. A study [12] reported that the carbonation resistance of slag concrete is even lower than the fly ash concrete. Another study [23] indicated that significant impairment towards carbonation resistance can already be observed at replacement percentage as low as 10%.

Research on concrete containing lime however, showed a more promising outcome with more results that are supportive towards the improvement of carbonation resistance emerged [1,25,27,28,31,33,35]. Even so, just as fly ash, there seems little direct correlations between the amounts of replacement with the pro- or anti-filler effect. This is true since some studies [1,25,31] indicated that high replacements (50% and more) are required to achieve the filling effect, while others [27,28,35] indicated the otherwise. Even in the studies that showed anti-filler effect [8,10,16,20,26,29,30,32,34], the replacement percentage has little to do with the outcome. This has led this study to believe that given a proper treatment, lime has a potential to be used as filler even at lower dosage. The aforementioned studies utilized the lime in its final form which is calcium carbonate. Calcium carbonate is inert filler and possess little to no hydration property such as the cement. Hence, the potential filling effect is limited by the position at which these inert filler particles reside within the concrete. If more of it happened to reside within the capillary chambers, than filler affect may be observed. Conversely, if more of these inert particles reside within the gel itself or stuck in the aggregate pores, than the filling effect would have been wasted. Hence, the occurrence of the Dispersion Paradox phenomenon described in [27].

It is the continuous hydration of the cement that makes the concrete increase in strength overtime due to the gel growth and densification that will ultimately filling the void within the binder matrix. This gel growth phenomenon inspired this study to emulate it in other form and this is where this study differs in the method of lime utilization and is explained later in this section. Rust inhibitors that depend on cathodic/anodic/cathodic-anodic reactions can protect the steel bar from corrosion but not without sacrifice on cost and additional subject matter expert employment. This is because there are many types of corrosion inhibitors that can be browsed through the market such as organic, inorganic, combination of organic-inorganic, water-based and coating which all have their respective purposes and correct methods of applications. On top of that, research on corrosion inhibitors generally focus on eliminating chloride elements and hydrochloric acid [37]. As to whether or not the inhibition mechanisms work similarly in carbonation rich environment is unknown. The use of rust inhibitor focusses on projects with special requirements such as underground and offshore structures exposed to aggressive chloride environment [37] and certainly not for all-purpose use for just any projects. This is shown in a series of test conducted by [36] which indicated that at given circumstances, calcium nitrate based inhibitors failed to perform its task but alkanolamine based inhibitor did success. Hence, rust inhibitor may not be an option for many projects.

In light of the highlighted issues along with other out of scope factors, sustainability has become the spotlight for contingency plans throughout the world. In Malaysia, Ministry of Energy, Green Technology and Water, has outlined the 2017 national Green-Technology Policy [40] that encourages people to consume more on the renewable natural resources as an alternative to the non-renewable natural resources apart from emphasizing construction and building sustainability. This is where the wasted mussel shells fit in the research design of this study.

The chemistry of concrete carbonation relies on the diffusion of carbon dioxide gas into the hardened binder. To inhibit corrosion due to carbonation, method to isolate the chemical interaction has to be devised and this can be achieved by applying the pro-filler principle of the lime in the aforementioned studies. In this study, a counter-intuitive approach designed to use the carbonation itself to inhibit the carbonation process is proposed. This design is called as the self-suffocation method in which the lime in its designed intermediate form shall hinder the carbon dioxide flux as the carbonation process proceeds.

Lime has a much higher mass unit than the quicklime or slaked lime. In atomic scale, higher mass unit is normally associated with higher atomic radii. This study postulates that the resulting higher atomic radii imposes a volumizing effect. Since the carbon dioxide flux proceeds via the capillarity matrix, there is a maximum 80% probability that this volumizing effect happens within [41]. This research named the material of interest as the Post-morph Lime Filler (PLF). The idea behind the naming of “Post-morph” comes from the expected behavior of the quicklime and slaked lime upon carbonation. The lime crystals will only morphed once the concrete is exposed to carbonation. Contrary to many other researchers that incorporate the lime during concrete mixing, this research incorporates the quicklime instead. The term “Post-morph” indicates that the actual lime will only be autogenously deposited after the exposure. The amount of deposition strictly dependent of the degree of carbonation. By designing the mechanism of interaction in this way, the natural carbonation process is fully taken advantage of.

2. MATERIAL PREPARATION AND METHODS

The mussel shell sample were obtained from the Danga River. The shells were washed using tap water and manually soaked with a brush to remove stubborn impurities. The cleaned shells were then air dried for a few days before being oven dried at 105°C for 24 hours to remove pore humidity. The shells were then isothermally heated at 1000°C for 1 hour to remove carbon dioxide from the calcium carbonate. The calcined shells were left to cool for several hours to the room temperature before being subjected to milling process for 1 hour. The milled calcined shell was sifted to pass the 63 µm aperture and the samples were then considered ready for experimentations. However, some experimentations did used some samples that were not calcined.

Mix design was prepared using the Department of Environment method (DOE) [42] with a target 28th day mean strength of 35MPa (standard deviation, s of 3.05). Concretes were made from Tasek (Malaysia) brand CEM1 OPC (grade 42.5), crushed granites with 20 mm maximum size, crushed quarry sand (33.3% passing the 600 µm mesh) and tap water. Mixing was done using a rotary mixer with feeding sequence of water, cement+PLF mixture, sand and finally granites. Mixing time followed recommendation from [43]. Table 1 shows the mix design for the control and the PLF concretes.

Table 1: Concrete mix design

Cube size	100 x 100 x 100 mm			
Characteristic strength	30 MPa			
Target mean strength (28th day)	35 MPa			
Margin	Within 1.64s			
w/c	0.6			
Replacement groups	Control	PLF5	PLF7.5	PLF10
Cement (kg/m³)	360	342	333	324
PLF (kg/m³)	0	18	27	36
Water (kg/m³)	216			
Sand (kg/m³)	967			
Granite (kg/m³)	857			
Conditioning	Plastic sheathing for 6 and 27 days at room temperature and humidity.			

2.1 Methods

The beginning part of the study focused more on the fundamental and metallurgic analyses which includes particle dispersion, mineralogy and crystallography. Then the focusing shifted to the study of the effect of aforementioned fundamentals in civil engineering aspect which includes carbonation and microstructure analysis.

2.1.1 Particle Dispersion

Two groups of materials were given focus for particle size distribution analysis and they were the OPC and the PLF itself. The test was conducted using CILAS1180 laser diffraction machine at room temperature of 25 °C and a mean relative humidity of 65±3%. Distilled water was used as dispersing agent and 5-10 grams of samples were prepared for each group.

2.1.2 Chemical and Mineralogical Analyses

Three materials were tested for either their chemical or mineralogical or both compositions. They are the OPC, un-calcined mussel shell, and calcined mussel shell (including PLF). All the tested samples were in powdered form and sieved to pass the 63 µm aperture. XRD analysis was carried out using the Bruker D8 diffractometer, scanned between 10° – 90° Bragg angle with step of 0.02° and X-ray wavelength (λ) of 1.5406 angstrom (Å). The chemical and minerals were determined using the Evaluation (EVA) software and some match analyses were doubly verified using Crystallographic Open Database (COD).

The XY coordinates of the obtained diffractograms were used to perform computerized Gaussian fitting. This is a specialize technique applied to only the un-calcined mussel shell diffractogram in this study to perform the crystallite size measurement. Gaussian fitting was conducted to execute measurements of the Full Width at Half Maximum (FWHM) of the selected peaks with the most pronounced intensity. The components of the FWHM were obtained from Snyder and Jenkins [44]. The obtained components of the FWHM are transferred into a spreadsheet software to perform the necessary crystallite size measurement using the Scherer's equation shown in the Eq. (1) below where d is the diameter of the crystallite measured in Angstrom (Å), K is the correction factor which is typically taken as 1 for spherical shape assumption, λ is the wavelength of the x-ray measured in Angstrom (Å), B is the FWHM converted in radians and $\cos(\theta_B)$ is the cosine of the angle of B measured also in radians.

$$d = \frac{K \lambda}{B \cos(\theta_B)} \quad (1)$$

The crystallite sizes were used to give a rough estimation of the crystal packing efficiency by comparing the median particle size (D_{50}) obtained via the particle size distribution (PSD) analysis, and the amount of crystallite needed to match the longest span (median diameter) of the particle. This was done using Eq. (2).

$$\text{Amount of crystallite} = \frac{D_{50}}{d_m} \quad (2)$$

Further justifications were made by using 2-dimensional draws of the involved crystal systems in the un-calcined mussel shell. Modelling of any crystal structure was made using the Visualization for Electronic and Structural Analysis (VESTA) software version 3.4.7.

2.1.3 Carbonation

Method for testing concrete carbonation was adapted from three standards which are the BS EN 14630 (Determination of carbonation depth in hardened concrete by the phenolphthalein method) [45], the BS EN 13295 (Determination of resistance to carbonation) [46] and the BS EN 12390 – 10 (Determination of the carbonation resistance at atmospheric levels of carbon dioxide) [47]. The exposure was conducted for 6 months at intervals of 60, 90, 120 and 180 days.

Four groups of concrete were assigned and they were the control group, and concretes containing 5% (PLF5), 7.5% (PLF7.5) and 10% (PLF10) replacements. This test was performed in a natural environment (exposed to ambient air but sheltered from rain). The exposure to the environmental carbon dioxide (CO₂) at 0.0552% (552 ppm) begun after the 27th day of curing in the plastic wrap.

Three environmental parameters were recorded on daily basis which are the concentration of the carbon dioxide gas, relative humidity and ambient temperature. In the three aforementioned standards for the carbonation testing, the carbon dioxide gas concentration is to be recorded three times a day, whereas the ambient relative humidity value has to be recorded at least once a day for as long as the carbonating testing proceeds.

The carbonation depth of each and every carbonated face were taken in the form of mean average. The test was carried out by pressing the concrete cube in between two metal bars using a hydraulic compression machines and carbonation depth was measured using a digital Vernier caliper. The depth of the natural carbonation follows the square root of time function as stated by [47] and was used in this study to obtain the carbonation coefficient. The square root of time function is shown in Eq. (3) where D: depth of carbonation in millimeter, k: carbonation coefficient in (mm/√year), and t is time in years.

$$D = \frac{k}{\sqrt{t}} \quad (3)$$

2.1.4 FESEM and EDX

The analyses were performed using the Jeol JSM 7600F. All samples were coated with Aurum (Au)/gold to enhance conductivity. The 2-dimensional SEM image of the interest topography was subjected to a specialized contouring technique that caused it to become 3-dimensional. This is done to give the actual in-depth view of the topography through a more sophisticated approach. Any other 3-dimensional objects such as the representation of particle grains were also made possible through graphical enhancement. The capillarity network of the concretes were compared to observe the volumizing effect of the PLF at high level magnifications. Elemental mapping was also made possible through the complementary EDX.

3. RESULTS AND DISCUSSION

This subtopic contains the outcomes of the conducted analyses. Note that the diffractogram from mineralogical analyses of the tested materials are compiled in a single diffractogram for easier comparison.

3.1 Particle Dispersion

Laser diffraction indicated that the prepared mussel shell ash particle dispersion resembles to that of the OPC's (Fig. 1). The median particle diameter (D₅₀) of the PLF is 19.69 μm which is approximately 23% larger than the OPC's. The typical median average

(D₅₀) size of the OPC can be as low as 10-15 μm [48] and may go as high as 10-20 μm [49]. The tested OPC and PLF average sizes are tally with the statements in [48] and [49]. However, it is important to also note that in order to achieve a good PLF particle dispersion amongst the OPC's, median size (D₅₀) may not be as important as concentration. Ideally, the incorporation of PLF into the cement through replacement, will naturally increases and decreases certain range of available particle sizes. Since it is impossible to know which exact particle size were omitted and which were included, it has become an uncertainty. Hence, analysis should focus more on the entire sets of size through the dispersion curve rather than a single number like the D₅₀.

The tested particle dispersion of cement containing 5%, 7.5% and 10% PLF exhibited overlapping curves with each other within the upper limit (OPC) and lower limit (PLF) curves. Hence, they are not included due to repetition of considerably identical patterns but suffice to say that the incorporation of the PLF into the cement at 10% maximum did not alter the original OPC particle dispersion significantly. This suggest that within 10% dosage, the PLF particle can be in homogeny (disperse properly) with the OPC particle. Hence, maximizing the filler effect across the binder region of the concrete.

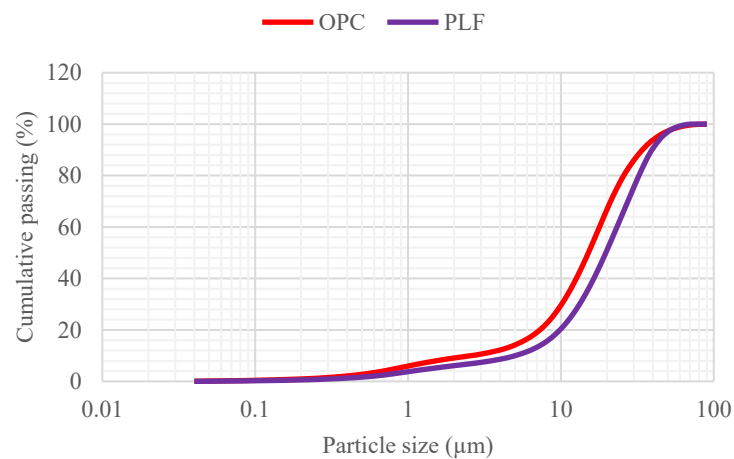


Fig. 1: Particle distribution curve of OPC and PLF.

3.2 Ordinary Portland Cement Mineralogy

Estimations that have been made through the matching of these signatures in EVA and COD give out the percentage of Bogue compositions as 59% for tricalcium silicate, 25.9% for dicalcium silicate, 1.6% tricalcium aluminate, 9.7% calcium aluminoferrite and 3.8% gypsum. The estimated amount of tri- and di- calcium silicates and calcium aluminoferrite are in a good agreement with the values reported by Santhakumar [50] which stated that the amount of the tricalcium silicate in OPC should varies in the range of 30-50%. Whereas, dicalcium silicate varies in the range of 20-45%. Calcium aluminoferrite should varies in the range of 6-10%. However, the calcium aluminate content in the tested OPC was found to be below average with the typically reported range of 8-12%. The gypsum amount is within the tolerated zone of 2-4%.

3.3 Mussel Shell (un-calcined form) Mineralogy

Diffraction pattern (*refer Fig. 8 at later page*) of the un-calcined mussel shell powder indicates that it contains largely calcium carbonate with orthorhombic crystal system. Orthorhombic profile in calcium carbonate compound is characteristic to aragonite polymorph which is highly anticipated in the shell of carbonate secreting organisms such as

the mollusk [51]. There are some traces of rhombohedral system which is characteristic to calcium carbonate of the calcite polymorph. According to Boggs [51], calcite is the most stable form of calcium carbonate which may take some amount of time to transform from the original aragonite arrangement.

The diffractogram peaks (Fig. 8) indicate that the tested sample are highly crystalline in regards to the very slim full-width at half maximum (FWHM) intensity [52]. Slim FWHM is also an indication of large crystallites [52]. Even with very slim FWHM, it is still considered a polymeric (crystal-amorphous) system nonetheless since perfect crystal would be impossible to obtain from the nature, but with a stressed minimum degree of amorphousness. As such, crystallite size measurement through the Scherer equation is made possible and shown in Table 2 whereas Fig. 2 shows the schematic diagram of the crystallites in a single particle grain of the micron size (drawn not to scale). Based on Fig. 2(a), one particle grain of mussel shell powder has a median diameter (D_{50}) of $19.69 \mu\text{m}$ as determined through the Cilas 1180 Particle Size Analyzer (PSA). A single particle grain contains hundreds if not, thousands of crystallites that are nano in size as shown in Fig. 2(b). This study believes that the amount of these nano crystallites present in a known grain diameter, can be taken advantage of for an indirect and qualitative density measurement.

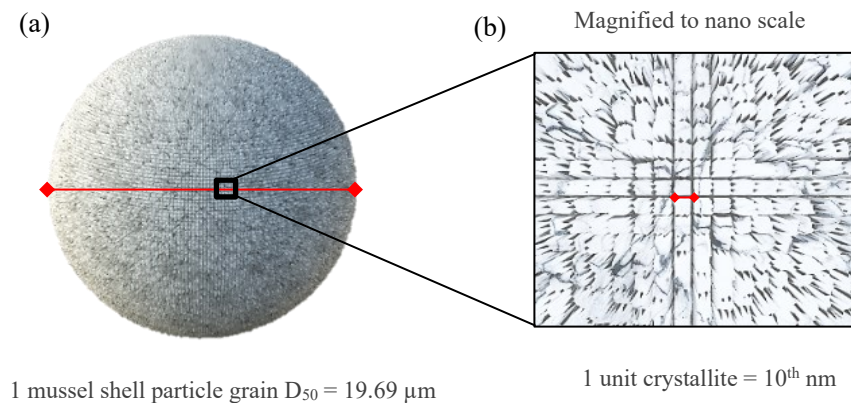


Fig. 2: Schematic diagram (a) particle grain (b) crystallites.

Based on Table 2, the mean sizes of the aragonitic and calcitic crystallites are 44.56 nm and 37.54 nm respectively. Some minor amount of peaks cannot be analyzed due to poor Gaussian fitting and skipped. Nevertheless, the data indicated that the present aragonitic crystallite in the tested sample is 18.7% smaller than the calcitic crystallite. By using this information, and considering two mussel shell particle grains, one is composed of pure aragonite, while the other is composed of pure calcite, a qualitative estimation of the crystal packing efficiency can be made. Using equation (2), the amount of crystallite that exist along the longest path of the particle can be predicted. Figure 3 shows the calculation of the diameter and crystallite packing.

Based on Fig. 3(a), if one mussel shell particle of $19.69 \mu\text{m}$ in diameter is made up of entirely aragonite crystal, there would be approximately 525 unit of aragonitic crystallite along the red line shown in Fig. 3(a). Likewise, if the same particle is made up of entirely calcite crystal instead, there would be approximately 442 unit of calcitic crystallite along the red line shown in Fig. 3(b). This indicates that for a fixed 2-dimension, aragonitic crystallite can be packed much more than the calcitic crystallite. In simple words, aragonite crystal can be denser than the calcite crystal. This is tally with the reported density values

of both crystals which happened to be at 2.94 g/cm^3 for aragonite [53] and 2.72 g/cm^3 for calcite [52].

Table 2: Components of the Scherer equation for crystallite size measurement of the mussel shell sample

Peak	Poly-morph	FWHM	2-Theta	Theta	FWHM(rad)	Theta (rad)	d (Å)	d (nm)	d (µm)
1	Ara	0.14886	26.21726	13.10863	0.002598097	0.22878875	547.9539	54.7954	0.0548
2	Ara	0.15146	27.23282	13.61641	0.002643476	0.23765119	539.6825	53.9683	0.0540
3	Cal	0.13587	31.10151	15.55076	0.002371379	0.27141188	606.9149	60.6915	0.0607
4	Ara	0.16921	33.11591	16.55796	0.002953272	0.28899083	489.8041	48.9804	0.0490
5	Ara	0.21286	36.09764	18.04882	0.003715108	0.31501134	392.532	39.2532	0.0393
6	Cal	0.19361	37.87276	18.93638	0.003379132	0.33050218	433.8019	43.3802	0.0434
7	Ara	0.31042	38.56152	19.28076	0.005417851	0.33651274	271.1277	27.1128	0.0271
10	Cal	0.19877	42.91974	21.45987	0.003469191	0.37454539	429.4441	42.9444	0.0429
11	Ara	0.2348	45.86098	22.93049	0.004098033	0.40021255	367.3733	36.7373	0.0367
12	Cal	0.27871	48.39646	24.19823	0.004864407	0.42233879	312.496	31.2496	0.0312
13	Ara	0.25499	50.23365	25.11683	0.004450415	0.43837129	344.0885	34.4089	0.0344
14	Ara	0.25583	52.42184	26.21092	0.004465076	0.45746685	346.1201	34.6120	0.0346
15	Ara	0.27972	52.9827	26.49135	0.004882035	0.46236128	317.3275	31.7327	0.0317
16	Ara	0.32815	66.02007	33.01004	0.005727298	0.5761338	288.6959	28.8696	0.0289
17	Ara	0.42884	69.00089	34.50045	0.00748467	0.60214636	224.7855	22.4786	0.0225
Mean calcite crystallite size (d_m)								44.56	0.04456
Mean aragonite crystallite size (d_m)								37.54	0.03754

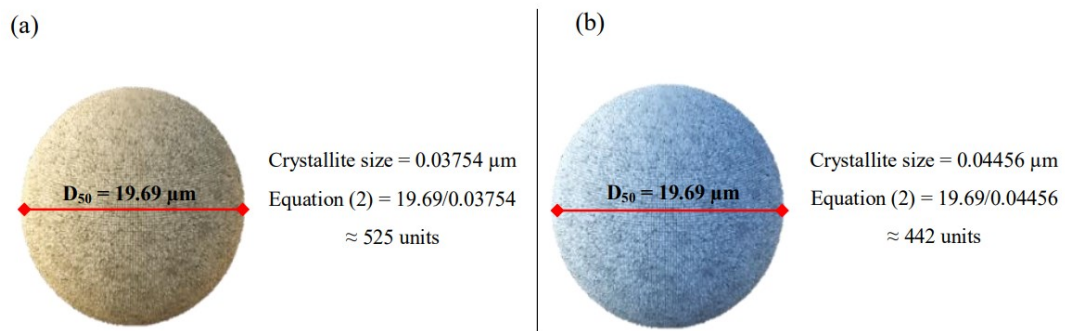


Fig. 3: Mussel shell crystallites unit measurements (a) only an aragonite particle composition, (b) only a calcite particle composition.

Comparing the density of these crystals with the density of a hardened normal concrete which typically stood at 2.3 g/cm^3 (converted from 2300 kg/m^3), it can be said that the packing of both crystals is higher than the concrete (27.8% and 18.3% higher respectively). This finding suggests that both type of these calcium carbonate polymorphs (aragonite and calcite) potentially possess densifying attribute when used in concrete.

In the view of this study, in regards to the packing efficiency of the said crystal systems, the densely packed aragonitic crystallite is due to the basis arrangement itself which revealed to be orthorhombic system through the XRD analysis. According to Wahab [54], orthorhombic system has a higher degree of freedom along the lattice axes such that $a \neq b \neq$

c. Considering crystal habit phenomenon during the formation of the aragonite itself, the crystallite can arrange themselves in every axes with multiple combinations of number a, b and c while maintaining the orthorhombic profile since a, b and c do not strictly need to be the same. Hence, the crystal can easily pack themselves. Contrary to the rhombohedral (hexagonal) arrangement of the calcite in which $a = b \neq c$. Two axes have to have equal dimension which result to a limited (rigid) possible crystal arrangement during the formation of the calcite. This is shown in the software-generated and -modified crystals of aragonite and calcite based on the models of Antao and Hassan [55] and Graf [56] respectively. The crystals with polyhedral views are plotted over their own respective 3x2 lattices in Fig. 4. Within the the same lattice size, it can be seen that the arrangement of the calcite (Fig. 4(b)) is more geometric and rigidly spaced compared to the aragonite structure (Fig. 4(a)). On the contrary, the packing of aragonite crystals can be seen denser than the calcite crystals. This further validates previous discussions by this study.

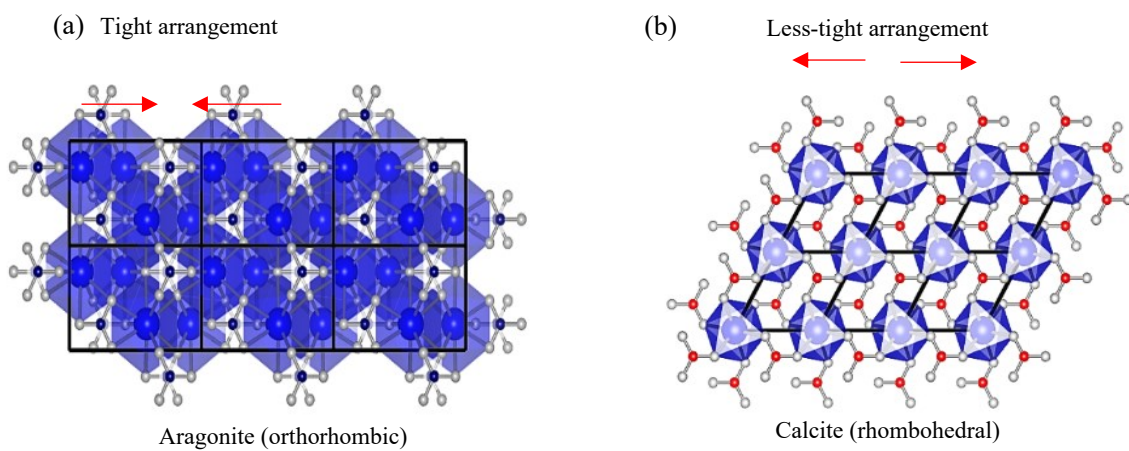


Fig. 4: Crystal structural arrangements (a) aragonite and (b) calcite.

According to Moore [57] and Haldar [58], calcite polymorph arrangement is thermodynamically stable at atmospheric level of pressure and temperature compared to aragonite. This means that it stays on being calcitic as long as not being subjected to geological event that leads to immense pressurization, water movement and temperature rise. It is due to this stability as well that cause calcite to become practically insoluble in water compared to aragonite. In the view of this study, by taking advantage of this calcite attribute, combined with proper adjustment to the degree of densification through dosage control, outward migration of the lime from concrete capillarity due to fluid movement can be hindered. Fluid movement, especially rain penetration can potentially migrate or wash off filler material at surface level. Thus, reducing its efficacy. This however, requires further studies and development.

Figure 5 shows the image of the shell magnified through the electron microscope at x5.0k zoom. The 2-dimensional image (Fig. 5(a)) has been processed into 3-dimensional figure (Fig. 5(b)) using a specialized technique to have a real and in-depth view of the topographic profile of the un-calcined shell. Local chemical constituents that are present have also been determined through the complementary energy-dispersive equipment. Based on Fig. 5(a), the topographic profile of the un-calcined mussel shell is revealed to be plates of flaky shape. The plates are more pronounced in the rendered 3-dimensional image (Fig. 5(b)). The plates are multi-layered which suggest the multi-stages of shell development throughout the life-span of the mussel. The platy profile is tally with the previous discussion

that indicates the presence of orthorhombic crystal system that is characteristic to the aragonite polymorph of the calcium carbonate.

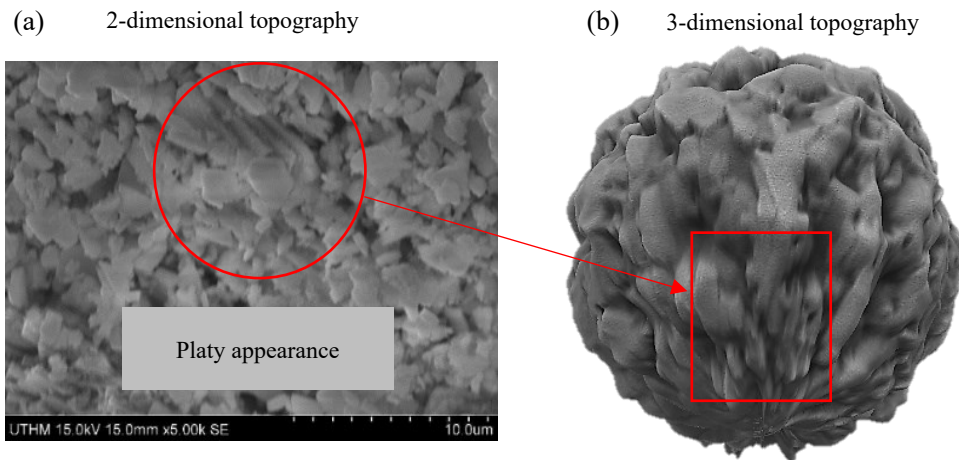


Fig. 5: Topographic profiles of the un-calcined mussel shell (a) 2-dimensional topography (b) 3-dimensional topography.

The platy profile of the un-calcined shell can also be observed in the findings from the previous studies [51,54,59,60]. The redundant proves in several studies signal the agreement of the presence of orthorhombic crystal system mentioned in this article that is characteristic to the aragonite polymorph of the calcium carbonate [61]. Orthorhombic system is basically an overextended version of a cubic system over two sides which resulted to a rectangular shape and if sufficiently thin, may assume platy appearance. Despite the known petrological knowledge that the existence of aragonite polymorph in normal environment is rare [57], these studies indicated that it is indeed possible via bio-mineralization process by these carbonate secreting organisms such as mussels and oysters. Whatever differences in the outcome of research that focus on the utilization of the un-calcined versus calcined shell husk in concrete may owed to this crystallographic variety. Hence, the significance of this piece of information. Since studies on concrete filler through crystallography point of view is largely insufficient, this particular finding may spark more attention.

3.4 Mussel Shell (Calcined Form) Mineralogy

Diffraction pattern of the calcined mussel shell sample indicated 90.61% match as calcium oxide profile and 76.1% match as calcium hydroxide profile as determined from the Crystallography Open Database (COD). Analysis has estimated the proportions of the compound as 93.6% CaO and 6.4% Ca(OH)₂. This study suspect that the minuscule presence of the calcium hydroxide is due to the hydration of the calcined mussel shell ash when it is exposed to the environmental humidity during the experimentation. No traces of calcium carbonate can be seen and this signify the effectiveness of the calcining method practiced in this study.

In regards to the exposure time during the experimentation, logically the calcium oxide should react with the environmental carbon dioxide to produce calcium carbonate as mentioned by Santhakumar [50]. Still, no traces of calcium carbonate due to this phenomenon has been detected either. This finding suggest that the rate of hydration is faster than the rate of carbonation. It has been further theorized by this study that the level of carbon dioxide concentration (0.0552%) versus the level of relative humidity concentration (>60%) may have a direct influence in the speed of reaction between the two.

The calcined mussel shell which is technically calcium oxide, is the first intermediate product formed during the high temperature treatment. This is followed by the second intermediate product which is the calcium hydroxide formed during the concrete mixing activity when the intermixed cement-calcined mussel shell ash reacts with the added water. This is verified through the live-image during hydration that was captured using a digital camera that was attached to an optical microscope which showed the characteristic hexagonal morphology of the calcium hydroxide (Fig. 6(a) and (b)). This is also observed under SEM microscopy (Fig. 7) and has been also crossed verified with other study [62].

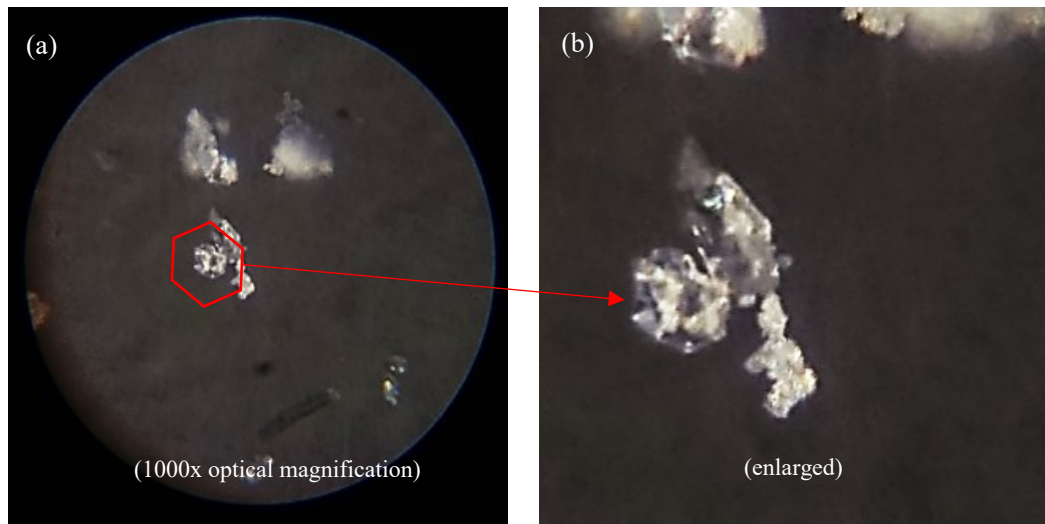


Fig. 6: Micrograph of the calcium hydroxide crystal exposed to visible spectrum wavelength (a) at 1000x (b) enlarged (zoom-in).

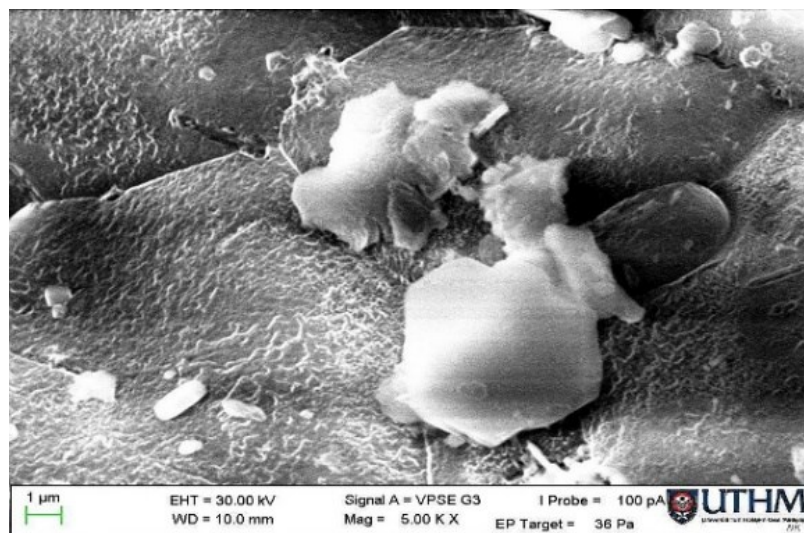


Fig. 7: SEM image of calcium hydroxide crystal exposed to X-ray spectrum wavelength.

Figure 8 summarized the diffractograms of the mussel shell at different stages. Based on Fig. 8, the last stage (Post-morphing) was tested at 180 days and it was found that a large portion of the calcium hydrate (CH) remained un-carbonated. There are two hypothetical statements that may be associated with this phenomenon. First, based on the evidence from the microstructure analysis, calcium carbonate appears to engulf the surrounding area where it has grown. This may create a layer of canopy or a blanket that shielded the underneath

and deeper CH from reacting with the carbon dioxide gas at surface level. More evidence linking to the blanket appearance of lime is portrayed in several other literatures [63,64]. Second, the degree of carbonation may simply has not reach a substantial level to convert a major amount of CH. It is also interesting to note that lime that was originally of the aragonitic system turned out to be calcitic after calcination and re-carbonation for 180 days. This is tally with the statement by Boggs [51]. However, this study is yet to fully understand the cause of this event but suffice to say, that the polymorph of these two crystals may change under certain circumstances even though they were once come from the same material. Hence, the importance of conducting more future studies on this particular subject.

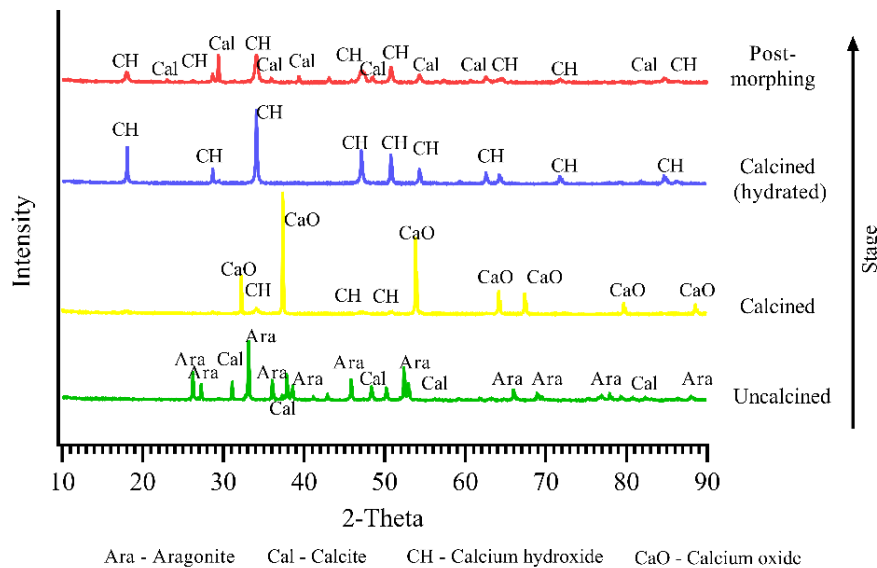


Fig. 8: Summary of mussel shell chemical and mineralogical analyses at different stages.

3.5 Carbonation

The obtained (actual) data are paired against theoretical (calculated) data using the model described in [65]. They are found to correlate positively and are in high agreement (R^2 approaching 0.9 and above). However, replacement percentage of PLF is inversely proportional to the correlation agreement value. This outcome suggests that, at a sufficiently high amount of replacement, the commonly used carbonation estimation model may no longer be valid. As for the scope of this study, it can be seen that 10% replacement exhibit a signal of downtrend in the R^2 where the value is marginally reaching 0.9 (Fig. 9(d)). This signify the limit of replacement where the model described in Neville [65] may stay true. It was found that the average carbonation depths of concrete containing the PLF are lower than the control concrete. Although, control concrete group in itself performed well below the typical carbonation coefficient range of 3-4 mm/ $\sqrt{\text{year}}$. The carbonation coefficient of the control concrete is at 2.92 mm/ $\sqrt{\text{year}}$ and this indicates a performance of better than average. The presence of the PLF improved the performance even more with a descending carbonation coefficient pattern across all experimental concrete samples. The carbonation coefficients of the PLF5, PLF7.5 and PLF10 are 1.83, 1.79 and 1.43 mm/ $\sqrt{\text{year}}$ respectively. Based on the coefficients, PLF10 concrete indicated the highest improvement which is up to a maximum of 51% lower carbonation coefficient compared to the control concrete. Figure 9 shows the correlational measurements of the actual and calculated data.

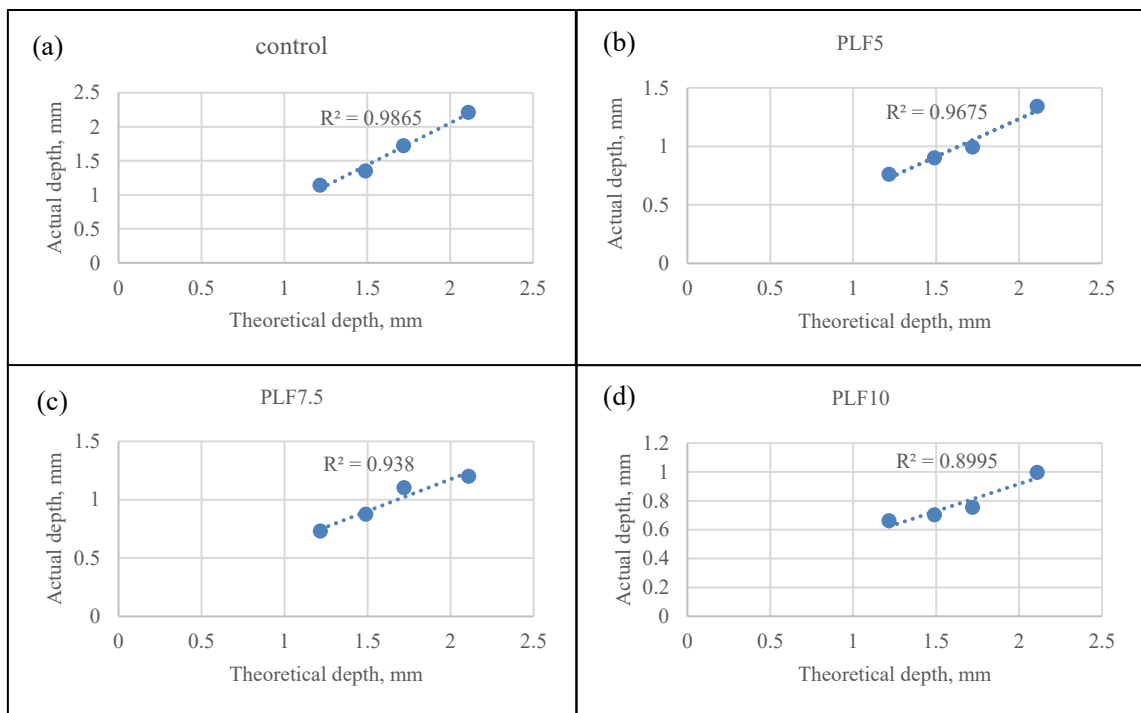


Fig. 9: Correlative measurement of the actual and theoretical data
 (a) control sample (b) at 5% of PLF (c) at 7.5% of PLF and (d) at 10% of PLF.

Incorporation of cementitious material greater than 5% interrupts the original requirement of CEM1 OPC which does not allow for such matter. Higher replacement than 5% will result to the reclassification into different cement class. Even so, if this limitation is to be considered, 5% incorporation of PLF already improves the carbonation coefficient by as much as 37% which is rather significant. Within the scope of this study, it seems possible to push replacement level beyond 5% limitation. Palm [66] showed that it is possible to incorporate high lime material (up to 50% replacement) while still keeping the carbonation performance on par with the control concrete. However, Palm [66] method required a proper water to cementitious ratio adjustment to achieve that. This is probably due to the different water demand for proper hydration when the cement is replaced at such a higher percentage. In the point of academics arguments, it is indeed possible. However, practical engineering knowledge may not allow for such a high replacement due to the need of balancing for other admixtures such as plasticizer, accelerator and water proofing. Hence, the method practiced in this study (lower replacement but better performance) has better advantage in terms of allocating rooms for other cementitious materials that are synonym in most civil engineering projects.

3.6 FESEM and EDX

Concrete samples containing PLF which were exposed to natural carbonation for 180 days with a mean CO₂ level of 552 ppm (global CO₂ baseline is 400 ppm) at a humidity of 60-75% and daily temperature of 28-34 °C, indicate lesser porosity compared to the control specimen. Figure 10 shows the FESEM image of the control and PLF5 concretes at a similar magnification of 2000x. The red lines are the capillarity of the concrete. The more of these line present, the more intense the capillary networks which are responsible for the overall porosity of the binder matrix. Only locations with deep fall were marked. Shallow falls were not considered as discontinuity since they may have just been variations in surface elevation. Concrete containing 5% (Fig. 10(b)) showed significantly lower discontinuity compared to

the control concrete (Fig. 10(a)) which may explain the lower carbonation depth in the phenolphthalein test, hence lower carbonation coefficient.

This study is confident that this phenomenon is contributed by the post-morphing of the PLF during exposure. Point-by-point surface elemental analysis of the specimen containing 5% PLF indicated the presence of all elements that make up the calcium carbonate which are calcium (Fig. 10(c)), carbon (Fig. 10(d)) and oxygen (Fig. 10(e)). No other unknown elements nor elements that are not indigenous to the original composition of a hardened concrete were detected except for aurum (Au) which is technically the gold coating, hence excluded.

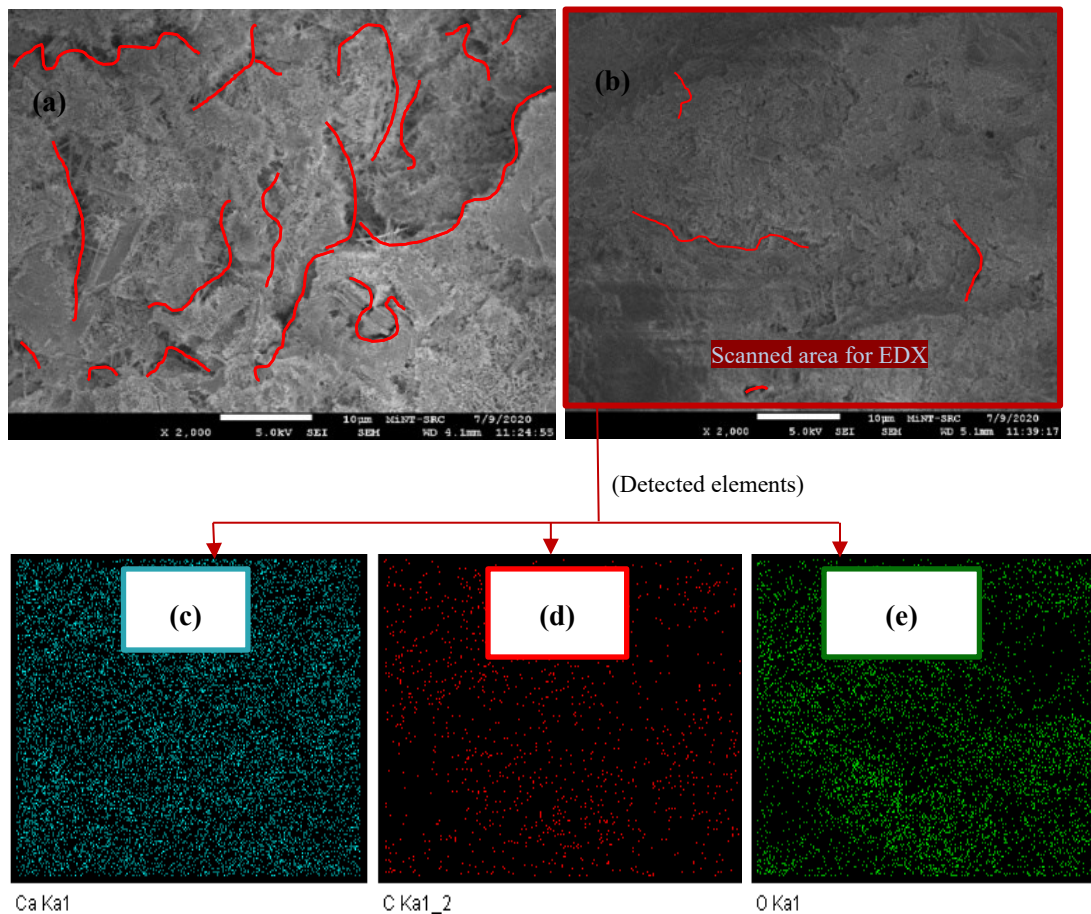


Fig. 10: Intensity of capillarity (a) control sample (b) sample with 5% PLF and surface elemental mapping (c) Calcium (d) Carbon (e) Oxygen.

In Fig. 11(a), it can be seen that at 8000x magnification, discontinuity, pores and typical hardened concrete products (CSH, ettringite, etc.) can clearly be seen. However, this is not the case for the PLF concretes especially for the PLF7.5 (Fig. 11(b)) and PLF10 (Fig. 11(c)) in which the typical products were not seen at the same level of magnification of 8000x. They are all concealed by the post-morphing of the lime. This is again verified by the EDX and the morphological images of the lime are identical across several other literatures such as those depicted by Chang [67] and Hamester [63]. Note that the flakes of lime in for PLF7.5 (Fig. 11(b)) is thinner than PLF10 (Fig. 11(c)). This is probably due to the lower concentration of the PLF. At lower concentration, the amount of carbonate minerals may not be sufficient to form the 3-dimensional structure vividly. If a sufficiently high concentration of carbonate mineral is present, the geometric arrangement of $a = b \neq c$ stated

in [51] becomes more pronounced such as in PLF10 (Fig. 11(c)) and hence, emanating cuboidal and “boxy” features across the surface.

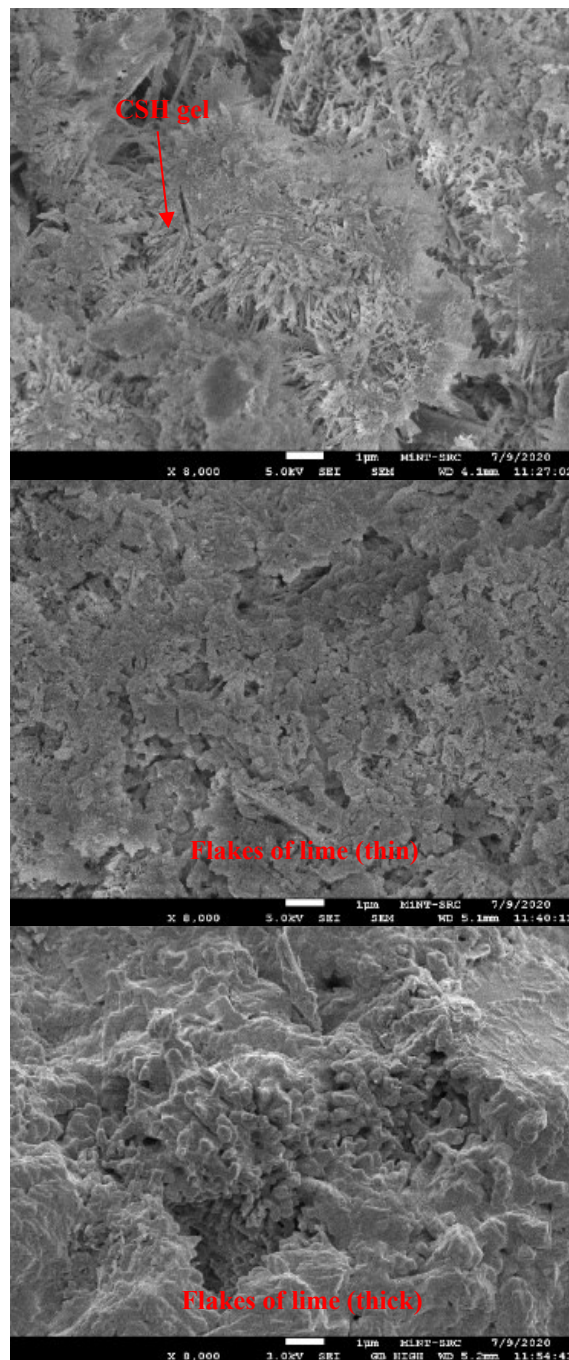


Fig. 11: PLF’s filler effect that enclosed (blanket) the concrete surface (a) control sample (b) sample with 7.5% PLF and (c) sample with 10%PLF.

4. CONCLUSIONS

Based on the conducted experiments, several conclusions can be deduced;

- Mussel shells are composed of aragonitic calcium carbonate in which the crystal system may change to calcitic under certain condition.

- Both aragonitic and calcitic calcium carbonate are denser (27.8% and 18.3% respectively) than concrete, hence their high potential as filler materials.
- Aragonite is denser than calcite due to its close-pack crystal arrangement.
- Concrete containing up to 10% PLF showed significantly lowered carbonation coefficient (up to 51%) and lower intensity of capillarity.
- FESEM analysis provided an incontrovertible evidence that the mussel shell ash (PLF) has clogged up the experimental concrete pores which was not found within the control sample.

ACKNOWLEDGEMENT

The authors acknowledge funding from the research grant Vot No. H353, received from the Research Management Centre (RMC) for the Universiti Tun Hussein Onn Malaysia (UTHM) for the success of this research works.

REFERENCES

- [1] Sideris KK, Anagnostopoulos NS. (2013) Durability of normal strength self-compacting concretes and their impact on service life of reinforced concrete structures. *Construction and Building Materials*, 41: 491–497. <https://doi.org/10.1016/j.conbuildmat.2012.12.042>
- [2] Phung QT, Maes N, Jacques D, Bruneel E, Van Driessche I, Ye G, De Schutter G. (2015) Effect of limestone fillers on microstructure and permeability due to carbonation of cement pastes under controlled CO₂ pressure conditions. *Construction and Building Materials*, 82: 376–390. <https://doi.org/10.1016/j.conbuildmat.2015.02.093>
- [3] Rezvani M, Proske T. (2017) Influence of chemical-mineralogical properties of limestone on the shrinkage behaviour of cement paste and concrete made of limestone-rich cements. *Construction and Building Materials*, 157: 818–828. <https://doi.org/10.1016/j.conbuildmat.2017.09.101>
- [4] Ekolu SO. (2016) A review on effects of curing, sheltering, and CO₂ concentration upon natural carbonation of concrete. *Construction and Building Materials*, 127: 306–320. <https://doi.org/10.1016/j.conbuildmat.2016.09.056>
- [5] Shibata T. (2002) Cost of corrosion in Japan. *Corrosion Science & Technology*, 31(2): 97–102.
- [6] Benítez P, Rodrigues F, Talukdar S, Gavilán S, Varum H, Spacone E. (2019) Analysis of correlation between real degradation data and a carbonation model for concrete structures. *Cement and Concrete Composites*, 95: 247–259. <https://doi.org/10.1016/j.cemconcomp.2018.09.019>
- [7] Nakai A, Imamoto K, Kiyohara C, Sato S, Tanaka A, Niwano K, Amemiya S. (2013) Influence of Finishing Materials on Carbonation Suppression of Concrete in Existing Structure. RILEM International Workshop on Performance-Based Specification and Control of Concrete Durability, 377–384.
- [8] Lollini F, Redaelli E, Bertolini L. (2016) A study on the applicability of the efficiency factor of supplementary cementitious materials to durability properties. *Construction and Building Materials*, 120: 284–292. <https://doi.org/10.1016/j.conbuildmat.2016.05.031>
- [9] Bogas JA, Real S, Ferrer B. (2016) Biphasic carbonation behaviour of structural lightweight aggregate concrete produced with different types of binder. *Cement and Concrete Composites*, 71: 110–121. <https://doi.org/10.1016/j.cemconcomp.2016.05.006>

- [10] Mohammed MK, Dawson AR, Thom NH. (2014) Carbonation of filler typed self-compacting concrete and its impact on the microstructure by utilization of 100% CO₂ accelerating techniques. *Construction and Building Materials*, 50: 508–516. <https://doi.org/10.1016/j.conbuildmat.2013.09.052>
- [11] Singh N, Singh SP. (2016) Carbonation resistance and microstructural analysis of Low and High Volume Fly Ash Self Compacting Concrete containing Recycled Concrete Aggregates. *Construction and Building Materials*, 127: 828–842. <https://doi.org/10.1016/j.conbuildmat.2016.10.067>
- [12] Shah V, Bishnoi S. (2018) Carbonation resistance of cements containing supplementary cementitious materials and its relation to various parameters of concrete. *Construction and Building Materials*, 178: 219–232. <https://doi.org/10.1016/j.conbuildmat.2018.05.162>
- [13] Li Z, Li S. (2018) Carbonation resistance of fly ash and blast furnace slag based geopolymer concrete. *Construction and Building Materials*, 163: 668–680. <https://doi.org/10.1016/j.conbuildmat.2017.12.127>
- [14] Marques PF, Chastre C, Nunes Â. (2013) Carbonation service life modelling of RC structures for concrete with Portland and blended cements. *Cement and Concrete Composites*, 37(1): 171–184. <https://doi.org/10.1016/j.cemconcomp.2012.10.007>
- [15] Tekin I, Yasin Durgun M, Gencil O, Bilir T, Brostow W, Hagg Lobland HE. (2017) Concretes with synthetic aggregates for sustainability. *Construction and Building Materials*, 133: 425–432. <https://doi.org/10.1016/j.conbuildmat.2016.12.110>
- [16] Proske T, Hainer S, Rezvani M, Graubner CA. (2014) Eco-friendly concretes with reduced water and cement content - Mix design principles and application in practice. *Construction and Building Materials*, 67(part C): 413–421. <https://doi.org/10.1016/j.conbuildmat.2013.12.066>
- [17] Harilal M, Rathish VR, Anandkumar B, George RP, Mohammed MSHS, Philip J, Amarendra G. (2019) High performance green concrete (HPGC) with improved strength and chloride ion penetration resistance by synergistic action of fly ash, nanoparticles and corrosion inhibitor. *Construction and Building Materials*, 198: 299–312. <https://doi.org/10.1016/j.conbuildmat.2018.11.266>
- [18] Cui D, Bantia N, Wang Q, Sun W. (2019) Investigation on porosity of partly carbonated paste specimens blended with fly ash through dual CT scans. *Construction and Building Materials*, 196, 692–702. <https://doi.org/10.1016/j.conbuildmat.2018.11.156>
- [19] Esquinas AR, Ledesma EF, Otero R, Jiménez JR, Fernández JM. (2018) Mechanical behaviour of self-compacting concrete made with non-conforming fly ash from coal-fired power plants. *Construction and Building Materials*, 182: 385–398. <https://doi.org/10.1016/j.conbuildmat.2018.06.094>
- [20] Bucher R, Diederich P, Escadeillas G, Cyr M. (2017) Service life of metakaolin-based concrete exposed to carbonation: Comparison with blended cement containing fly ash, blast furnace slag and limestone filler. *Cement and Concrete Research*, 99: 18–29. <https://doi.org/10.1016/j.cemconres.2017.04.013>
- [21] Carević V, Ignjatović I, Dragaš J. (2019) Model for practical carbonation depth prediction for high volume fly ash concrete and recycled aggregate concrete. *Construction and Building Materials*, 213: 194–208. <https://doi.org/10.1016/j.conbuildmat.2019.03.267>
- [22] Younsi A, Turcry P, Ait-Mokhtar A, Staquet S. (2013) Accelerated carbonation of concrete with high content of mineral additions: Effect of interactions between hydration and drying. *Cement and Concrete Research*, 43(1): 25–33. <https://doi.org/10.1016/j.cemconres.2012.10.008>
- [23] Yagüe A, Valls S, Vázquez E, Albareda F. (2005) Durability of concrete with addition of dry sludge from waste water treatment plants. *Cement and Concrete Research*, 35(6): 1064–1073. <https://doi.org/10.1016/j.cemconres.2004.07.043>

- [24] Sideris KK, Tassos C, Chatzopoulos A, Manita P. (2018) Mechanical characteristics and durability of self compacting concretes produced with ladle furnace slag. *Construction and Building Materials*, 170: 660–667. <https://doi.org/10.1016/j.conbuildmat.2018.03.091>
- [25] Palm S, Proske T, Rezvani M, Hainer S, Müller C, Graubner CA. (2016) Cements with a high limestone content - Mechanical properties, durability and ecological characteristics of the concrete. *Construction and Building Materials*, 119: 308–318. <https://doi.org/10.1016/j.conbuildmat.2016.05.009>
- [26] El-Hassan H, Shao Y. (2015) Early carbonation curing of concrete masonry units with Portland limestone cement. *Cement and Concrete Composites*, 62: 168–177. <https://doi.org/10.1016/j.cemconcomp.2015.07.004>
- [27] Hussin MH, Othman NH, Wan Ibrahim MH. (2019) Carbonation of concrete containing mussel (*Perna viridis*) shell ash. *Journal of Engineering, Design and Technology*, 17(5): 904–928. <https://doi.org/10.1108/JEDT-12-2018-0228>
- [28] Phung QT, Maes N, Jacques D, Bruneel E, Van Driessche I, Ye G, De Schutter G. (2015) Effect of limestone fillers on microstructure and permeability due to carbonation of cement pastes under controlled CO₂ pressure conditions. *Construction and Building Materials*, 82: 376–390. <https://doi.org/10.1016/j.conbuildmat.2015.02.093>
- [29] Lollini F, Redaelli E, Bertolini L. (2014) Effects of portland cement replacement with limestone on the properties of hardened concrete. *Cement and Concrete Composites*, 46: 32–40. <https://doi.org/10.1016/j.cemconcomp.2013.10.016>
- [30] Río O, Nguyen VD, Nguyen K. (2015) Exploring the potential of the functionally graded SCCC for developing sustainable concrete solutions. *Journal of Advanced Concrete Technology*, 13(3): 193–204. <https://doi.org/10.3151/jact.13.193>
- [31] Rezvani M, Proske T. (2017) Influence of chemical-mineralogical properties of limestone on the shrinkage behaviour of cement paste and concrete made of limestone-rich cements. *Construction and Building Materials*, 157: 818–828. <https://doi.org/10.1016/j.conbuildmat.2017.09.101>
- [32] Courard L, Michel F. (2014). Limestone fillers cement based composites: Effects of blast furnace slags on fresh and hardened properties. *Construction and Building Materials*, 51: 439–445. <https://doi.org/10.1016/j.conbuildmat.2013.10.076>
- [33] Valcuende, M., & Parra, C. (2010). Natural carbonation of self-compacting concretes. *Construction and Building Materials*, 24(5), 848–853. <https://doi.org/10.1016/j.conbuildmat.2009.10.021>
- [34] Meddah MS, Lmbachiya MC, Dhir RK. (2014) Potential use of binary and composite limestone cements in concrete production. *Construction and Building Materials*, 58: 193–205. <https://doi.org/10.1016/j.conbuildmat.2013.12.012>
- [35] Tsivilis S, Batis G, Chaniotakis E, Grigoriadis G, Theodossis D. (2000) Properties and behavior of limestone cement concrete and mortar. *Cement and Concrete Research*, 30(10): 1679–1683. [https://doi.org/10.1016/S0008-8846\(00\)00372-0](https://doi.org/10.1016/S0008-8846(00)00372-0)
- [36] Dhouibi L, Triki E, Raharinaivo A. (2002) The application of electrochemical impedance spectroscopy to determine the long-term effectiveness of corrosion inhibitors for steel in concrete. *Cement and Concrete Composites*, 24(1): 35–43. [https://doi.org/10.1016/S0958-9465\(01\)00062-2](https://doi.org/10.1016/S0958-9465(01)00062-2)
- [37] Dariva CG, Galio AF. (2014) Corrosion inhibitors—principles, mechanisms and applications. *Developments in corrosion protection*, 16: 365–378. <http://dx.doi.org/10.5772/57255>
- [38] Possan E, Thomaz WA, Aleandri GA, Felix EF, dos Santos ACP. (2017) CO₂ uptake potential due to concrete carbonation: A case study. *Case Studies in Construction Materials*, 6: 147–161.
- [39] Oliveira TV, Nogueira AA. (2016) Analysis of development of carbonation and surface wear of the concrete: a case study in Ship Lock 1 of the transposition system of Tucuruí dam. *Journal of Building Pathology and Rehabilitation*, 1(1): 1–8. <https://doi.org/10.1007/s41024-016-0019-0>

- [40] Ministry of Energy, Green Technology and Water (2017), Green Technology Masterplan Malaysia 2017-2030. Malaysia.
[https://doi.org/ISBN NO. 978-967-5893-09-4](https://doi.org/ISBN%20NO.%20978-967-5893-09-4)
- [41] Hussin MH. (2018) Keupayaan kadar pengkarbonatan konkrit campuran abu kulit kupang sebagai bahan gantikan separa simen. Master thesis, Universiti Tun Hussein Onn Malaysia, Department of Civil Engineering.
- [42] Teychenné DC, Franklin RE, Erntroy HC. (1997). Design of normal concrete mixes. Building Research Establishment Ltd, 331(1): 46.
- [43] Shalon R, Reinitz RC. (1958) Mixing time of concrete: technological and economic aspects. Building Research Station.
- [44] Jenkins R, Snyder RL. (1996) Introduction to X-ray Powder Diffractometry. In Introduction to X-ray Powder Diffractometry. John Wiley.
<https://doi.org/10.1002/9781118520994>.
- [45] British Standards Institution. Determination of Carbonation Depth in Hardened Concrete by the Phenolphthalein Method. London, BS EN 14630. 2006
- [46] British Standards Institution. Determination of Resistance to Carbonation. London, BS EN 13295. 2004
- [47] British Standards Institution. Determination of the Carbonation Resistance at Atmospheric Levels of Carbon Dioxide. London, BS EN 12390 – 10. 2017
- [48] Mehta PK, Monteiro PJM. (2006) Third Edition Prentice- Hall, Inc., Englewood Cliffs, NJ. In Concrete: microstructure, properties, and materials.
- [49] Khankhaje E, Hussin MW, Mirza J, Rafieizonooz M, Salim MR, Siong HC, Warid MNM. (2016) On blended cement and geopolymer concretes containing palm oil fuel ash. *Materials and Design*, 89: 385–398. <https://doi.org/10.1016/j.matdes.2015.09.140>
- [50] Santhakumar AR. (2007) Concrete technology. Oxford University Press.
- [51] Boggs S. (2009) Petrology of sedimentary rocks, second edition. In Petrology of Sedimentary Rocks, Second Edition (2nd ed., Vol. 9780521897167). Cambridge University Press. <https://doi.org/10.1017/CBO9780511626487>.
- [52] Waseda Y, Muramatsu A. (2004) Morphology control of materials and nanoparticles: advanced materials processing and characterization. Berlin. Springer-Verlag.
- [53] Klein and Dutrov (2008). The 23rd Edition of the Manual of Mineral Science (23rd ed.). Hoboken, NJ. Wiley J.
- [54] Wahab MA. (2009) Essentials of Crystallography. Oxford. Alpha Science International.
- [55] Antao SM, Hassan I. (2010) Temperature dependence of the structural parameters in the transformation of aragonite to calcite, as determined from in situ synchrotron powder X-ray-diffraction data. *Canadian Mineralogist*, 48(5): 1225–1236. <https://doi.org/10.3749/canmin.48.5.1225>
- [56] Graf DL. (1961) Crystallographic tables for the rhombohedral carbonates. *American Mineralogist*, 46: 1283–1316.
- [57] Haldar SK. (2020) Introduction to Mineralogy and Petrology (2nd ed.). Elsevier. <https://doi.org/10.1016/C2012-0-03337-6>
- [58] Moore CH. (2001) Developments in Sedimentology. Elsevier.
- [59] Buasri A, Chaiyut N, Loryuenyong V, Worawanitchaphong P, Trongyong S. (2013) Calcium oxide derived from waste shells of mussel, cockle, and scallop as the heterogeneous catalyst for biodiesel production. *The Scientific World Journal*, 2013. <https://doi.org/10.1155/2013/460923>
- [60] Hossain A, Bhattacharyya SR, Aditya G. (2015) Biosorption of cadmium by waste shell dust of fresh water mussel *lamellidens marginalis*: Implications for metal bioremediation. *ACS Sustainable Chemistry and Engineering*.
<https://doi.org/10.1021/sc500635e>
- [61] Monneron-Gyurits M, Joussein E, Soubrand M, Fondanèche P, Rossignol S. (2018) Valorization of mussel and oyster shells toward metakaolin-based alkaline activated material. *Applied Clay Science*, 162: 15–26.
<https://doi.org/10.1016/j.clay.2018.05.027>

- [62] Rochelle CA, Czernichowski-Lauriol I, Milodowski AE. (2004) The impact of chemical reactions on CO₂ storage in geological formations: A brief review. Geological Society, London, Special Publications, 233(1): 87-106.
- [63] Hamester MRR, Balzer PS, Becker D. (2012) Characterization of calcium carbonate obtained from oyster and mussel shells and incorporation in polypropylene. Materials Research, 15(2): 204–208. <https://doi.org/10.1590/S1516-14392012005000014>
- [64] Hossain MZ. (2013) Waste Shell Husks Concrete: Durability, Permeability and Mechanical Properties. Journal of Building Construction and Planning Research, 01(03): 61–66. <https://doi.org/10.4236/jbcpr.2013.13009>
- [65] Neville AM. (2011) Properties of concrete (5th ed.). England. Longman.
- [66] Palm S, Proske T, Rezvani M, Hainer S, Müller C, Graubner CA. (2016) Cements with a high limestone content - Mechanical properties, durability and ecological characteristics of the concrete. Construction and Building Materials, 119: 308–318. <https://doi.org/10.1016/j.conbuildmat.2016.05.009>
- [67] Chang JJ, Yeih W, Huang R, Chi JM. (2003) Mechanical properties of carbonated concrete. Journal of the Chinese Institute of Engineers, Transactions of the Chinese Institute of Engineers, Series A/Chung-Kuo Kung Ch'eng Hsueh K'an, 26(4): 513–522. <https://doi.org/10.1080/02533839.2003.9670804>